Korean J. Chem. Eng., 36(7), 1131-1139 (2019)
DOI: 10.1007/s11814-019-0290-2

pISSN: 0256-1115
eISSN: 1975-7220

Simultaneous desulfurization and denitrogenation of model fuels by polyethylene glycol-modified resorcinol/formaldehyde resin-derived carbon spheres

Jie Wen*,†, Dongdong Zhao*, Yingying Lu*, Jing Huang, Yanping Li*, Hui Zhang*,†, and Airong Li***

*College of Chemistry and Chemical Engineering, Oil & Gas Field Applied Chemistry Key Laboratory of Sichuan Province, Southwest Petroleum University, Chengdu, Sichuan 610500, China
**Department of Chemical Engineering, Sichuan University, Chengdu, Sichuan 610064, China
(*Received 23 January 2019 • accepted 28 April 2019*)

Abstract−A series of resorcinol/formaldehyde (RF) resin-derived carbon spheres modified by polyethylene glycol (PEG) were prepared. The effects of PEG addition time during hydrothermal treatment and molecular weight on the pore structure, surface acidic groups, particle size, and adsorption performances of the obtained spherical activated carbons were investigated. Two types of model fuel containing indole, quinoline, and dibenzothiophene (DBT) as target adsorbates were prepared to evaluate the adsorption performances of the spheres, which increased in the order of DBT<quinoline<indole. Hydrogen bonding may be critical in the removal of indole. Both the surface area and oxygen-containing functional groups influenced the adsorption capacity, with the latter significantly influenced by PEG addition time. PEG addition during the RF resin cross-linking stage sharply reduced the total concentration of acidic groups on the carbon sphere surfaces. The adsorption thermodynamics and kinetics of nitrogen and sulfur compounds were also investigated. The adsorption isotherms of all S/N species were of the Freundlich type at 25 °C. The pseudo-second-order rate equation well described the adsorption kinetics. Both external diffusion and intra-particle diffusion controlled the rate of adsorption.

Keywords: Phenolic Resin, Spherical Carbon, Polyethylene Glycol, Adsorption, Desulfurization and Denitrogenation

INTRODUCTION

As the demand for straight-run fuel oil has increased, natural resources of light crude oil, which is easily processed, are continuously decreasing, forcing most oil refineries to use more problem-fraught heavy oil [1]. Heavy oil has a high content of sulfur and nitrogen compounds, which produce SO_x and NO_x after combustion, causing serious environmental pollution. As a result, many countries have enacted fuel standards that limit the sulfur content of fuels [2,3]. Although nitrogen compounds are not similarly regulated, numerous studies have shown that their presence inhibits the removal of sulfur [4-6], making their removal likewise necessary [7]. However, traditional hydrodesulfurization (HDS) and hydrodenitrogenation (HDN) methods cannot easily meet the international community's new standards for transportation oil [8]. This is further complicated by the considerable amount of expensive hydrogen required for HDS and HDN. Additionally, the high temperatures and pressures necessary for catalytic hydrogenation reactions are also favorable for the hydrogenation of unsaturated hydrocarbons, which reduces the octane number of the oil [8]. Thus, the development of more effective and efficient desulfurization and denitrogenation approaches is crucial both environmentally and economically. The removal of sulfur and nitrogen compounds by adsorption has attracted widespread attention because of its low cost and high efficiency [9-13]. Moreover, the latest standards of transportation oil can be attained by employing adsorption processes before hydrogenation [14,15].

Activated carbon is an excellent adsorbent for desulfurization and denitrogenation as it has not only a large specific surface area but also rich surface functional groups [11,16-19]. Sano et al. [20] reported that activation with particular oxidants such as HNO_3, H_2SO_4, and H_2O_2, dramatically improved the adsorption capacity of activated carbon for nitrogen species by introducing the particular oxygen functional groups. Zhou et al. [21] also observed that oxidative modification of activated carbon by HNO_3 efficiently improved the adsorption performance for sulfur compounds, which could be attributed mainly to an interaction of the acidic oxygen containing groups on activated carbon with the sulfur compounds. Ania et al. [22] prepared a series of metal-loaded polymer-derived activated carbons and investigated their adsorption capacity for dibenzothiophene removal. The metals incorporated to the surface act not only as active sites for selective adsorption of sulfur compound, but also as catalyst initiators in reactive adsorption. Among activated carbons, carbon spheres have many additional advantages, such as smooth surfaces, uniform particle sizes, low flow resistance for gas or liquid adsorption, and high filling densities [23]. These properties have led to their wide application in fields including energy storage [24,25], electronics [26,27], environmental protection [28], biomedicine [29], and catalyst carrier technology [30]. However, few reports have explored the adsorptive denitrogenation and desulfurization properties of carbon spheres. Their adsorption properties have been demonstrated by Zhang et al. [31] in a study on the adsorptive removal of dibenzothiophene (DBT) with polyethylene glycol (PEG)-modified carbon spheres. However, only the effect of

†To whom correspondence should be addressed.
E-mail: wenjie@swpu.edu.cn, huizhang@swpu.edu.cn

PEG on the textural structure of the carbon spheres was discussed; the effect of additives on the oxygen-containing functional groups on the surface of the carbon spheres was not considered.

In this study, PEG-modified phenolic resin-based carbon spheres with largely microporous structures were prepared and employed in the removal of S/N compounds by adsorption from model fuels. When preparing the modified carbon spheres, the stage at which PEG was added and the PEG molecular weight were varied to investigate how they influenced the pore structure, surface functional groups, particle size, and adsorption performances of the carbon spheres. The adsorption isotherms and kinetics for both sulfur and nitrogen compounds were also studied.

EXPERIMENTAL

1. Synthesis of PEG-modified Phenolic Resin-based Carbon Spheres

Resin spheres were prepared through an extended Stöber method [32]. The hydrothermal treatment and modification procedure was as follows: a mixture of deionized water (416 mL) and absolute ethanol (1,040 mL) was prepared under continuous stirring. After more than 1 h, 5.2 mL of ammonia solution was added to the aqueous alcohol solution. After stirring for 30 min, 10.4 g of resorcinol and a certain amount of PEG were added, followed by 14.56 mL of formaldehyde, which was added dropwise. Subsequently, the prepared solution was heated to 30 °C and held for 24 h (addition reaction stage). A cloudy mixture was obtained that was subsequently heated to 100 °C in an autoclave under a N_2 atmosphere for a further 24 h (cross-linking stage). The resultant resin material was washed and then dried at 100 °C for 12 h. For carbonization, the resin material was heated to 350 °C at a rate of 1 °C·min^{-1} and held for 2 h in a tube furnace (OTF-1200X, Hefei Kejing Materials Technology Co., Ltd., China) under a N_2 atmosphere. Following this, the resin material was heated to 600 °C at a rate of 1 °C·min^{-1} and held for 4 h. About 12.7 g of the final carbon sample was attained. It was named $CS_{PEG[x]L}$, where [x] is the molecular weight of PEG and L indicates that the PEG was added before the low-temperature (30 °C) addition reaction stage. In a further experiment, PEG was instead added after the reaction stage, before transferring to the autoclave for cross-linking, with no other conditions changed. The obtained product was designated as $CS_{PEG[x]H}$, where H indicates that the PEG was added before the high-temperature stage (100 °C). For comparison, pure carbon spheres were synthesized without PEG and denoted as CS.

2. Characterization of Adsorbents

The surface areas of the carbon spheres were determined using a fully automated Brunauer-Emmett-Teller (BET) surface area and porosity analyzer (ST-MP-9, Quantachrome Instruments, USA) at −196 °C. The *t*-plot method was used to measure the micropore volumes, and the pore size distributions were estimated by density functional theory (DFT) calculations. Boehm titration was performed to determine the acidic oxygen-containing functional groups on the surface. NaOH was added to neutralize the carboxyl, lactonic, and phenolic groups on the surface of the carbon spheres. The quantity of NaOH consumed in each titration step was used to calculate the amount of the corresponding acidic oxygen-containing functional groups. Field-emission scanning electron microscopy (FESEM, Zeiss SUPRA 55VP, Germany) was used to characterize the morphologies of the sorbent materials.

Table 1. Composition of model fuel MF#1

Chemicals	Molar concentration (μmol·g^{-1})	S/N (ppmw)
S/N compound[a]	71.4	2285/1000
Octane	Balance	

[a]The S/N compound is quinoline, indole, or DBT. For isotherm study, the concentrations of quinolone, indole, and DBT were varied from 14.3 μmol·g^{-1} to 71.4 μmol·g^{-1}

Table 2. Composition of model fuel MF#2

Chemicals	Molar concentration (μmol·g^{-1})	S/N (ppmw)
Quinoline	71.4	1000
Indole	71.4	1000
DBT	71.4	2285
Octane	Balance	

3. Adsorption in Model Fuels

To evaluate the adsorption performance of the carbon spheres, two types of model fuels were prepared using quinoline, indole, and DBT as target compounds. Model fuel MF#1 contained one of these heterocyclic sulfur/nitrogen compounds, and MF#2 contained all three, as indicated by the compositions shown in Tables 1 and 2, respectively.

The adsorption experiments were performed by batch adsorption conducted in brown vials with vigorous stirring for 24 h. To determine the adsorption isotherms, solutions of a single nitrogen or sulfur compound at different molar concentrations were prepared. The molar concentrations were 14.3, 28.6, 42.9, 57.1, and 71.4 μmol·g^{-1} for quinoline and indole, and 14.3, 17.9, 23.8, 35.7, and 71.4 μmol·g^{-1} for DBT. The isotherm tests were conducted at 25 °C in a water bath. For kinetic study, the sorbent was soaked in

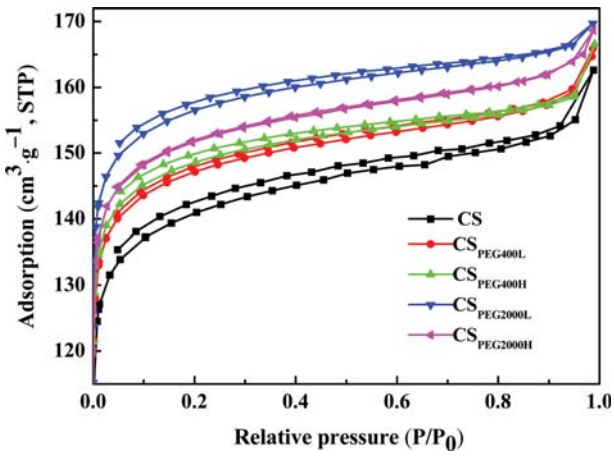

Fig. 1. Nitrogen adsorption-desorption isotherms of the pristine and PEG-modified carbon spheres.

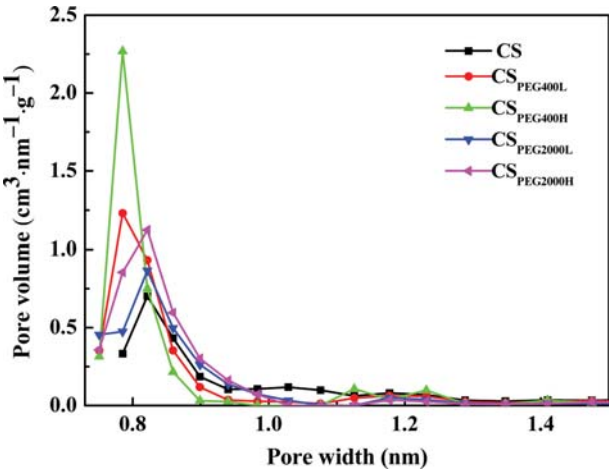

Fig. 2. Pore size distributions curves for the carbon spheres.

model fuel MF#1 and the fuel was sampled after different contact times. Gas chromatography (Varian GC450) was used to analyze the fuels' compositions after adsorption by using an internal standard (1,2,3,4-tetrahydeonaphthalene). Finally, the adsorption capacity was calculated.

Table 3. Structural parameters of the carbon spheres studied[a]

Sample	S_{BET} ($m^2 \cdot g^{-1}$)	V_t ($cm^3 \cdot g^{-1}$)	V_{mi} ($cm^3 \cdot g^{-1}$)	Pore size (nm)
CS	556.7	0.253	0.204	0.995
$CS_{PEG400L}$	585.3	0.257	0.221	0.785
$CS_{PEG400H}$	592.2	0.258	0.225	0.785
$CS_{PEG2000L}$	625.2	0.263	0.235	0.822
$CS_{PEG2000H}$	604.5	0.261	0.228	0.822

[a]S_{BET} is the BET surface area of the carbon sphere; V_t is the total volume; V_{mi} is the micropore volume determined by the *t*-plot method

RESULTS AND DISCUSSION

1. Pore Structures of Carbon Spheres

Fig. 1 shows the nitrogen adsorption-desorption isotherms of the pristine and PEG-modified carbon spheres. All the carbon adsorbents exhibit type I isotherms [33], indicating dominant microporous structures. Compared to those of the pristine carbon spheres CS, the nitrogen adsorption capacities of the modified samples were improved by the addition of PEG as a pore-forming agent, with $CS_{PEG2000L}$ showing the highest nitrogen adsorption capacity.

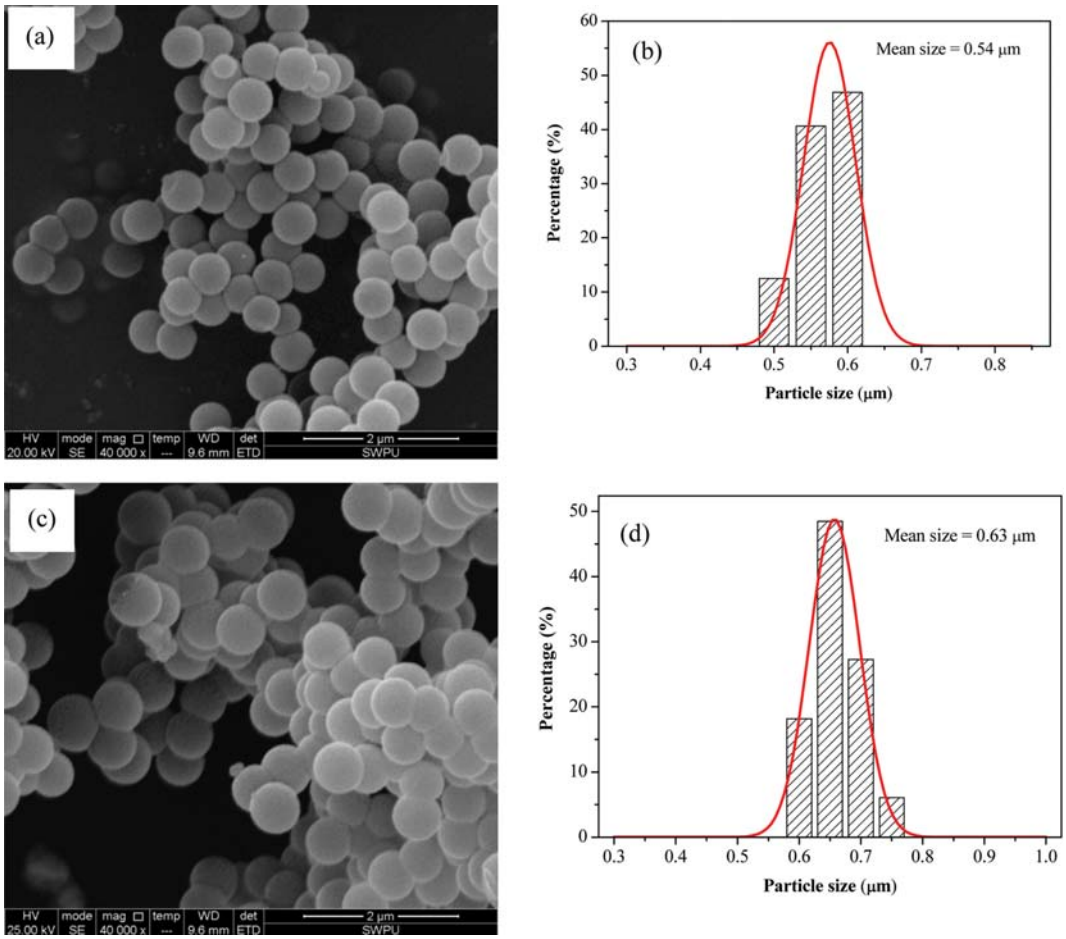

Fig. 3. SEM images and particle size distributions of carbon spheres: (a), (b) CS; (c), (d) $CS_{PEG400L}$; (e), (f) $CS_{PEG400H}$; (g), (h) $CS_{PEG2000L}$; and (i), (j) $CS_{PEG2000H}$.

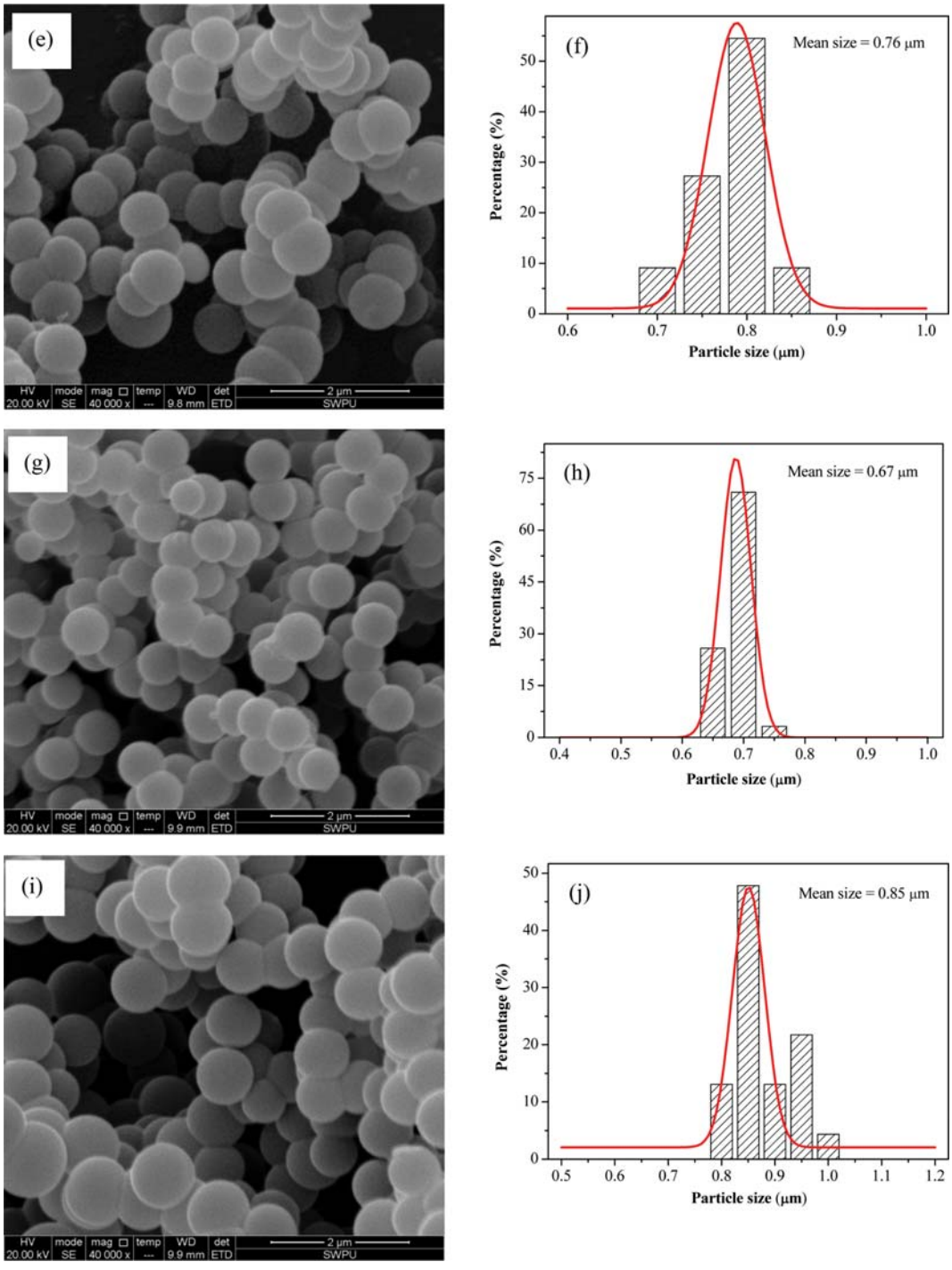

Fig. 3. Continued.

The pore-size distributions of the synthesized carbon spheres are shown in Fig. 2. The micropore diameter is mainly distributed around 0.8 nm, which ensure the adsorbate molecules are able to enter these pores for adsorption on the internal surface of carbon spheres [2,34]. The pore diameter of the modified carbon sphere is decreased after adding PEG400, compared to that of CS. The pore sizes of PEG400-modified CS are smaller than those of PEG2000-modified CS. Table 3 shows the textural parameters of the carbon adsorbents calculated from the nitrogen adsorption-desorption isotherms. Pristine CS has an average surface area of 556.7 $m^2 \cdot g^{-1}$ and a micropore volume (*t*-plot) of 0.204 $cm^3 \cdot g^{-1}$; both these values are improved by PEG modification, reaching maximum values of 625.2 $m^2 \cdot g^{-1}$ and 0.235 $cm^3 \cdot g^{-1}$, respectively, for $CS_{PEG2000L}$. The pore structure is changed by PEG modification because PEG decomposition induces micropore formation in the CS during carbonization. Moreover, the higher-molecular-weight PEG2000 improves the surface area and micropore volume, thus increasing the nitrogen adsorption capacity, to a greater extent than PEG400.

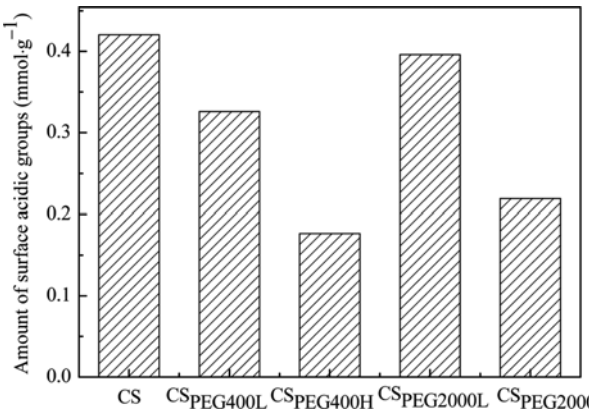

Fig. 4. Concentrations of acidic oxygen-containing functional groups determined by Boehm titration.

2. Morphology of Carbon Spheres

SEM images of the carbon spheres are displayed in Fig. 3. Uniform nanospheres with smooth surfaces are formed. The addition of PEG is observed to increase the particle size of the carbon spheres, with PEG2000 inducing a larger increase than PEG400. Furthermore, adding the pore-forming agent before the high-temperature stage is more effective for this particle size enlargement.

3. Acidic Oxygen-containing Functional Groups on Surfaces of Carbon Spheres

Fig. 4 shows the acidic oxygen-containing functional group concentrations on the sample surfaces, as determined by Boehm titration [35]. In general, the total concentration of surface acidic groups does not exceed 0.5 mmol·g^{-1}. However, $CS_{PEG400H}$ and $CS_{PEG2000H}$ show marked reductions in the content of surface acidic oxygen functional groups compared to $CS_{PEG400L}$ and $CS_{PEG2000L}$. Hence, introducing PEG before the high-temperature stage dramatically reduces the concentration of surface acidic groups, as confirmed by the adsorption results.

There are two main steps in the formation of the resin polymer spheres [32]. First, resorcinol reacts with formaldehyde at 30 °C to form hydroxymethyl-substituted species. Further cross-linking occurs during the hydrothermal treatment at 100 °C, yielding uniform colloidal spheres. When PEG is introduced before the high-temperature stage, numerous hydroxymethyl-substituted species with reticulate structures are interspersed with a large amount of PEG, which may participate in the polymerization of the hydroxymethyl-substituted species and subsequently reduce the number of surface acidic groups on the prepared carbon samples. In contrast, when PEG is added before the low-temperature stage, only a small amount becomes included in the carbon precursor, because PEG is interspersed among the resorcinol and formaldehyde monomers. This is in agreement with the particle sizes of the carbon spheres, which is increased slightly when PEG is added before the low-temperature stage, and significantly when the addition is performed before the high-temperature stage (Fig. 3).

4. Adsorption Performance

The adsorption capacities of the carbon spheres with model fuel MF#1 are shown in Fig. 5(a). The adsorption capacities are increased in the order of DBT<quinoline<indole for all the carbon

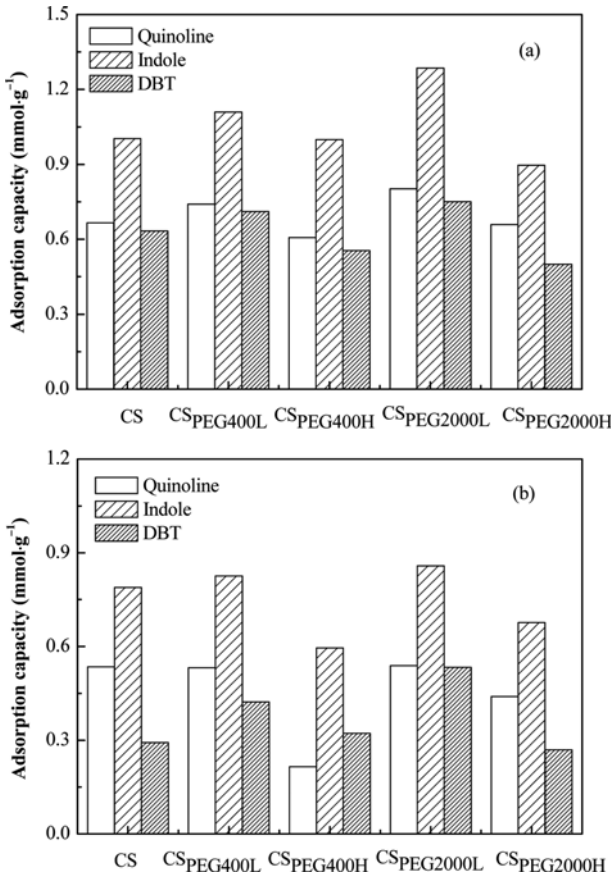

Fig. 5. Adsorption capacities of the carbon spheres for (a) model fuel MF#1 and (b) model fuel MF#2.

samples. The adsorption capacity of indole is the largest because it forms hydrogen bonds with both acidic and basic groups. Quinoline and DBT are basic and thus only interact with acidic groups. Furthermore, DBT is a 3-ring compound which increases internal mass transfer resistance due to big molecule. Therefore, the adsorption capacity of DBT is the lowest. $CS_{PEG400L}$ and $CS_{PEG2000L}$ show higher adsorption capacities than CS, whereas $CS_{PEG400H}$ and $CS_{PEG2000H}$ exhibit noticeably lower capacity, owing to the sharp reduction in the concentration of acidic groups on the carbon sphere surfaces [18]. The deterioration of adsorption capacity of $CS_{PEG400H}$ and $CS_{PEG2000H}$ can also be attributed to their significantly increased particle sizes, which increase the adsorbate diffusion path lengths. Furthermore, when added before the low-temperature stage, PEG2000 leads to slightly higher adsorption capacities than PEG400. Thus, $CS_{PEG2000L}$ demonstrates the highest adsorption capacity of 1.29, 0.75, and 0.64 mmol·g^{-1} for indole, quinoline, and DBT, respectively. As discussed earlier, the higher-molecular-weight PEG2000 improves the surface area and micropore volume, thus increasing the adsorption capacity, relative to PEG400. The adsorption capacity of sulfur and nitrogen compounds over $CS_{PEG2000L}$ obtained in this work is compared in Table 4 with the previously reported values achieved using metal organic frameworks (MIL-101-Cr) [36], activated carbon (PS-Cu) [22], and carbon sphere (ACS_{PEG35}) [31]. Compared with the adsorption capacity of the above adsorbents, the capacity of $CS_{PEG2000L}$ based on weight is lower.

Table 4. Comparison of the adsorption capacity on various adsorbents

Adsorbent	Surface area [$m^2 \cdot g^{-1}$]	Capacity based on weight [$mmol \cdot g^{-1}_{ad.}$]			Capacity based on surface area [$\mu mol \cdot m^{-2}$]			Ref.
		Indole	Quinoline	DBT	Indole	Quinoline	DBT	
MIL-101-Cr	2789	0.61	1.02	---	0.219	0.366	---	36
PS-Cu	566	---	---	3.60	---	---	6.360	22
ACS_{PEG35}	1501	---	---	0.72	---	---	0.480	31
$CS_{PEG2000L}$	625	1.29	0.75	0.64	2.064	1.200	1.024	This work

However, in comparison of the adsorptive capacity based on the surface area, as shown in Table 4, $CS_{PEG2000L}$ have much higher adsorptive capacity per square meter than MIL-101-Cr and ACS_{PEG35} for both sulfur and nitrogen compounds, implying that $CS_{PEG2000L}$ has better surface chemical property than MIL-101-Cr and ACS_{PEG35} [37]. PS-Cu adsorbent shows higher adsorption capacity per square meter for DBT than the present work, which is due to the loaded metal on activated carbon.

Model fuel MF#2 is adopted to evaluate the adsorption performance of the carbon adsorbents in a competitive adsorption system. The total adsorption capacity is significantly improved, because the total amount of sulfur and nitrogen compounds in MF#2 is three-times those in MF#1. $CS_{PEG2000L}$ shows the highest adsorption capacity of 1.85 $mmol \cdot g^{-1}$. When MF#2 is used as the feed, S comprises 19-29% of the total adsorbed S and N, in contrast to 33% in the initial composition. This seems to suggest that nitrogen compounds compete with sulfur for active sites of carbon spheres, and the carbon spheres favor adsorbing nitrogen compounds. Indeed, the selectivity for indole contributes 46-52% of the total adsorbed S and N.

5. Adsorption Isotherms and Kinetics

Model fuel MF#1 was prepared with different initial concentrations of the S and N species to study the adsorption isotherm of $CS_{PEG2000L}$ at 25 °C. Fig. 6 shows the effect of initial concentration, C_0, on the adsorption of S/N onto the carbon spheres. The equilibrium adsorption capacity of the three S/N compounds appears to linearly increase with the initial concentration, which indicates that the adsorption is concentration-driven [16]. The two nitrogen compounds display similar gradients, which are higher than that of the sulfur compound.

The Langmuir and Freundlich isotherm models are widely used to analyze equilibrium adsorption data. The model parameters and the statistical fits of the adsorption data obtained at 25 °C for the Langmuir and Freundlich equations are given in Table 5. The adsorption of quinoline, indole, and DBT follow the Freundlich model

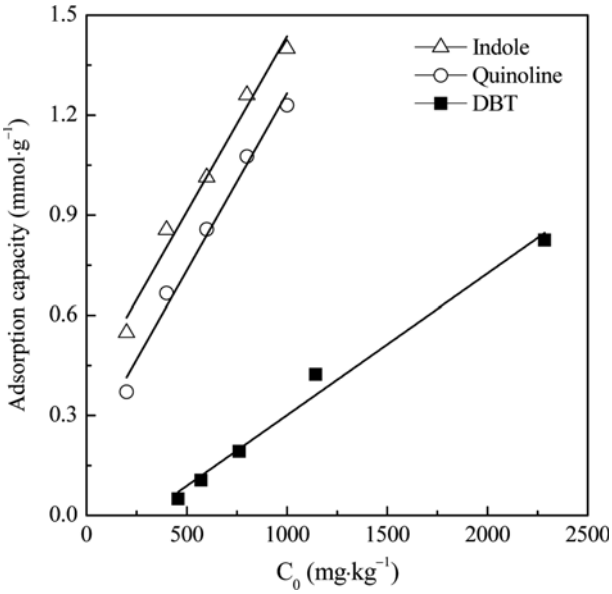

Fig. 6. Effect of initial concentration on equilibrium at 25 °C.

better than the Langmuir model. The condition 1/n<1 indicates physical nonlinear adsorption of the S or N species, because the adsorbent-adsorbate interaction decreases with increasing surface density [38]. The Freundlich isotherm indicates that the carbon spheres present highly heterogeneous surfaces in the adsorption of DBT, quinoline, and indole, as well as multilayer adsorption in which there is infinite surface coverage by the adsorbates without reaching a maximum.

Fig. 7 shows the effect of contact time on the removal of S/N compounds at room temperature and atmospheric pressure. Adsorption tests were performed by soaking $CS_{PEG2000L}$ in model fuel MF#1 for 24 h. The uptake of adsorbate species is rapid in the first

Table 5. Langmuir and Freundlich constants for $CS_{PEG2000L}$

	Langmuir			Freundlich		
	q_m ($mmol \cdot g^{-1}$)	K_L ($kg \cdot mg^{-1}$)	R^2	1/n	K_F ($mmol \cdot kg^{1/n} \cdot mg^{-1/n} \cdot g^{-1}$)	R^2
Indole	1.651	0.007260	0.9612	0.3728	0.1265	0.9873
Quinoline	2.036	0.002232	0.9806	0.6203	0.0226	0.9923
DBT	4.247	0.001333	0.7160	0.7634	0.0022	0.9651

K_L and q_m are Langmuir constants related to the energy of adsorption and maximum capacity, respectively; K_F and 1/n are Freundlich constants related to the adsorption capacity and intensity, respectively

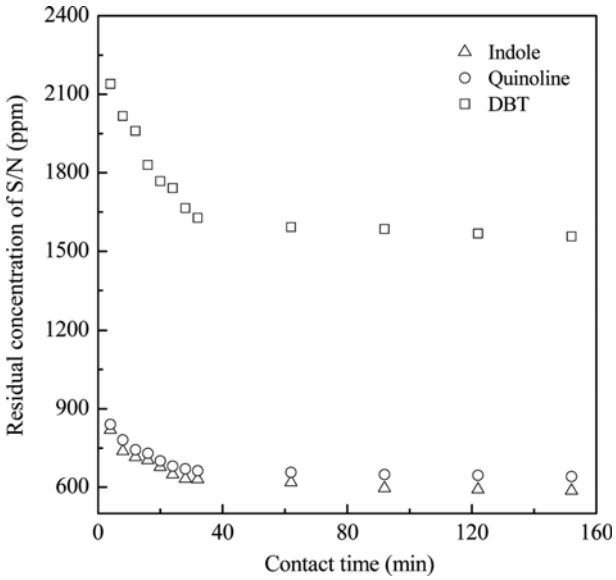

Fig. 7. Effect of contact time on the removal of S/N compounds.

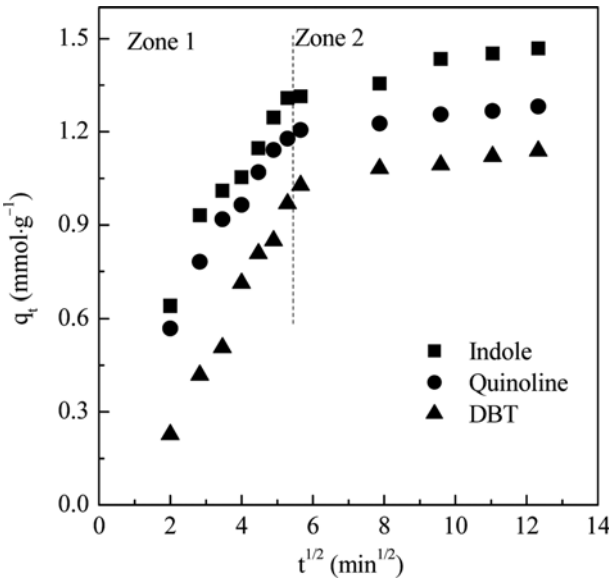

Fig. 8. Weber-Morris intra-particle diffusion plot for adsorption of S/N by phenolic resin-based carbon spheres.

30 min, with more than 90% of the equilibrium amount of S/N compounds being removed in this stage. The uptake becomes much slower thereafter, until equilibrium is approached after 150 min.

To further study the adsorption kinetics of S/N compounds on the modified carbon spheres, the more frequently used pseudo-first-order and pseudo-second-order kinetic models were applied to the adsorption results [39]. The results of fitting the experimental data with the pseudo-first-order and pseudo-second-order models are presented in Table 6. The correlation coefficients (R^2=0.99-1.00 for the pseudo-second-order model and R^2=0.86-0.92 for the pseudo-first-order model) demonstrate better correlation for the pseudo-second-order kinetic model, indicating that the adsorption of S and N compounds onto the carbon spheres follows the pseudo-second-order rate expression. Indole has a larger k_{2ad} value and a higher initial adsorption rate h than the other two components. Furthermore, the predicted equilibrium adsorption capacity for indole is the highest of the three compounds, which agrees with the experimental data. Kim et al. [37] also reported that activated carbon showed a higher adsorption selectivity for indole than for quinoline. The hydrogen bonding interaction may be important in the adsorptive removal of indole by the activated carbon.

Adsorption kinetics are typically controlled by various mechanisms such as film diffusion, pore diffusion, and adsorption on the sorbent surface [40]. To identify the mechanism involved in a particular adsorption process, the intra-particle diffusion model is often used. Intra-particle diffusion can be expressed by the Weber-Morris equation as [41]

$$q_t = k_{id} t^{1/2} + C \quad (1)$$

where k_{id} is the rate constant for intra-particle diffusion (mmol·g^{-1}·min$^{-1/2}$) and C is a constant related to the thickness of the boundary layer (mmol·g^{-1}).

Fig. 8 presents Weber–Morris plots of q_t vs. $t^{0.5}$ for S- and N-compound adsorption. There are two linear zones (zones 1 and 2) displayed for the adsorption process, which indicates that two successive adsorption steps exist in the uptake of S/N by the carbon spheres [42,43]. The initial linear portions do not pass through the origin, which means that intra-particle diffusion is not the only rate-controlling step in the S/N adsorption process [42,44]; film diffusion may also influence the S/N uptake. The second linear portion can be ascribed to intra-particle diffusion through the smaller micropores. The values of k_{id} and *C* estimated from Fig. 8 are listed in Table 7. The high correlation coefficients (R^2>0.95) indicate that the intra-particle diffusion model fits the experimental data well over the whole concentration range. The intercept value C provides information about the boundary layer thickness; namely, higher intercept values indicate enhanced boundary layer

Table 6. Adsorption kinetic models rate constants for different S and N compounds

Adsorbates	Pseudo-first-order		Pseudo-second-order			
	k_{1ad} (min^{-1})	R^2	k_{2ad} (mmol·g^{-1}·min^{-1})	R^2	h	$q_e{}^a$ (mmol·g^{-1})
Indole	0.0325	0.9211	0.1136	0.9997	0.2624	1.52
Quinoline	0.0329	0.8568	0.1611	0.9997	0.2807	1.32
DBT	0.0332	0.9028	0.0636	0.9948	0.0989	1.25

[a]Calculated by pseudo-second-order model

k_{1ad} and k_{2ad} are rate constants, h is the initial adsorption rate at $t \rightarrow 0$

Table 7. Intra-particle diffusion parameters for different adsorbates using $CS_{PEG2000L}$

Adsorbates	C (mmol/g)	Step I		Step II	
		k_{i1} (mmol·g^{-1}·min$^{-1/2}$)	R_1^2	k_{i2} (mmol·g^{-1}·min$^{-1/2}$)	R_2^2
Indole	0.33	0.187	0.962	0.024	0.952
Quinoline	0.24	0.180	0.982	0.010	0.988
DBT	−0.23	0.226	0.988	0.016	0.972

effects [43]. It is noteworthy that the obtained intercept for DBT is negative. This indicates that the thickness of the boundary layer retards intra-particle diffusion in the carbon sphere [45]. The slope of the linear portion k_{id} shows the rate of adsorption. The more gradual slope in the second part of the linear curve corresponds to a slower adsorption process, which is followed by the establishment of equilibrium.

CONCLUSIONS

PEG-modified spherical carbons derived from resin polymers were prepared and tested for the adsorption of indole, quinoline, and DBT. The addition of PEG increased both the specific surface area and micropore volume of the carbon spheres, with higher-molecular-weight PEG2000 being more effective than PEG400. However, the concentration of acidic groups on the surface of the spheres was significantly changed by varying the time of PEG addition during the hydrothermal treatment. Adding PEG at the RF resin cross-linking stage sharply reduced the concentration of acidic groups, which reduced the adsorption capacity for S- and N-containing compounds from model fuels. Correlation of the structural properties and the adsorption behavior of the carbon spheres revealed that S/N adsorption was dominated by the pore structure and surface chemistry of the carbon adsorbents. Therefore, $CS_{PEG2000L}$, in which PEG2000 was added at the resorcinol/formaldehyde addition stage, exhibited the highest adsorption capacity because the abundant micropores and surface acidic groups of this sample were the most favorable for S/N adsorption. The adsorption thermodynamics, studied by obtaining adsorption isotherms of the S and N compounds on $CS_{PEG2000L}$, were of the Freundlich type. The kinetic studies showed that the pseudo-second-order rate equation fitted the experimental data well; both external diffusion and intra-particle diffusion were controlling steps of the adsorption process.

ACKNOWLEDGEMENTS

This work was supported by the National Natural Science Foundation of China (No. 21206139 and No. 21606058).

REFERENCES

1. A. Stanislaus, A. Marafi and M. S. Rana, *Catal. Today*, **153**, 1 (2010).
2. C. O. Ania and T. J. Bandosz, *Langmuir*, **21**, 7752 (2005).
3. A. N. Zhou, X. L. Ma and C. S. Song, *J. Phys. Chem. B*, **110**, 4699 (2006).
4. H. Mizutani, H. Godo, T. Ohsaki, Y. Kato, T. Fujikawa, Y. Saih, T. Funamoto and K. Segawa, *Appl. Catal. A-Gen.*, **295**, 193 (2005).
5. H. Yang, J. W. Chen, Y. Briker, R. Szynkarczuk and Z. Ring, *Catal. Today*, **109**, 16 (2005).
6. X. J. Tao, Y. S. Zhou, Q. Wei, S. J. Ding, W. W. Zhou, T. T. Liu and X. H. Li, *Fuel*, **188**, 401 (2017).
7. G. C. Laredo, P. M. Vega-Merino, F. Trejo-Zárraga and J. Castillo, *Fuel Process. Technol.*, **106**, 21 (2013).
8. C. S. Vimal, *RSC Adv.*, **2**, 759 (2012).
9. M. Almarri, X. L. Ma and C. S. Song, *Ind. Eng. Chem. Res.*, **48**, 951 (2009).
10. H. Chen, Y. H. Wang, F. H. Yang and R. T. Yang, *Chem. Eng. Sci.*, **64**, 5240 (2009).
11. M. Seredych and T. J. Bandosz, *Energy Fuel*, **23**, 3737 (2009).
12. M. Maes, M. Trekels, M. Boulhout, S. Schouteden, F. Vermoortele, L. Alaerts, D. Heurtaux, Y.-K. Seo, Y. K. Hwang, J.-S. Chang, I. Beurroies, R. Denoyel, K. Temst, A. Vantomme, P. Horcajada, C. Serre and D. E. De Vos, *Angew. Chem. Int. Edit.*, **50**, 4210 (2011).
13. S. A. Shahriar, H. F. Lin and Y. Zheng, *Ind. Eng. Chem. Res.*, **51**, 14503 (2012).
14. Y. Sano, K. Sugahara, K.-H. Choi, Y. Korai and I. Mochida, *Fuel*, **84**, 903 (2005).
15. Y. Sano, K.-H. Choi, Y. Korai and I. Mochida, *Appl. Catal. B-Environ.*, **49**, 219 (2004).
16. J. Wen, X. Han, H. F. Lin, Y. Zheng and W. Chu, *Chem. Eng. J.*, **164**, 29 (2010).
17. X. Han, H. F. Lin and Y. Zheng, *J. Hazard. Mater.*, **297**, 217 (2015).
18. J. Wen, H. F. Lin, X. Han, Y. Zheng and W. Chu, *Ind. Eng. Chem. Res.*, **56**, 5033 (2017).
19. Y. X. Yang, G. Q. Lv, L. L. Deng, B. Q. Lu, J. L. Li, J. J. Zhang, J. Y. Shi and S. J. Du, *J. Clean. Prod.*, **161**, 422 (2017).
20. Y. Sano, K.-H. Choi, Y. Korai and I. Mochida, *Energy Fuel*, **18**, 644 (2004).
21. A. N. Zhou, X. L. Ma and C. S. Song, *Appl. Catal. B-Environ.*, **87**, 190 (2009).
22. C. O. Ania and T. J. Bandosz, *Carbon*, **44**, 2404 (2006).
23. J. Liu, N. P. Wickramaratne, S. Z. Qiao and M. Jaroniec, *Nat. Mater.*, **14**, 763 (2015).
24. C. Y. Shu, B. Song, X. D. Wei, Y. Liu, Q. Tan, S. K. Chong, Y. Z. Chen, X. D. Yang, W. H. Yang and Y. N. Liu, *Carbon*, **129**, 613 (2018).
25. X. T. Xu, Y. Liu, M. Wang, C. Zhu, T. Lu, R. Zhao and L. K. Pan, *Electrochim. Acta*, **193**, 88 (2016).
26. G. L. Wu, Y. H. Cheng, Z. H. Yang, Z. R. Jia, H. J. Wu, L. J. Yang, H. L. Li, P. Z. Guo and H. L. Lv, *Chem. Eng. J.*, **333**, 519 (2018).
27. R. Zhang, L.-X. Wang, Y.-D. Zhang, C.-H. Ge, J.-P. Wang, Y. Zhang and X.-D. Zhang, *J. Fluoresc.*, **28**, 439 (2018).
28. L. L. Zhou, G. L. Zhang, M. Wang, D. F. Wang, D. Q. Cai and Z. Y. Wu, *Chem. Eng. J.*, **334**, 400 (2018).

29. X. B. Zhang, Y. Y. Li, H. Lv, J. H. Feng, Z. Q. Gao, P. Wang, Y. H. Dong, Q. Liu and Z. D. Zhao, *Biosens. Bioelectron.*, **106**, 142 (2018).
30. Z. X. Wu, J. Wang, R. Liu, K. D. Xia, C. J. Xuan, J. P. Guo, W. Lei and D. L. Wang, *Nano Energy*, **32**, 511 (2017).
31. C. M. Zhang, W. Song, G. H. Sun, L. J. Xie, L. Wan, J. L. Wang and K. X. Li, *Ind. Eng. Chem. Res.*, **53**, 4271 (2014).
32. J. Liu, S. Z. Qiao, H. Liu, J. Chen, A. Orpe, D. Y. Zhao and G. Q. Lu, *Angew. Chem. Int. Edit.*, **50**, 5947 (2011).
33. S. Brunauer, L. S. Deming, W. E. Deming and E. Teller, *J. Am. Chem. Soc.*, **62**, 1723 (1940).
34. N. Li, J. Zhu, X. L. Ma, Q. F. Zha and C. S. Song, *AIChE J.*, **59**, 1236 (2013).
35. H. P. Boehm, *Carbon*, **32**, 759 (1994).
36. Y. Wu, J. Xiao, L. M. Wu, M. Chen, H. X. Xi, Z. Li and H. H. Wang, *J. Phys. Chem. C*, **118**, 22533 (2014).
37. J. H. Kim, X. L. Ma, A. N. Zhou and C. S. Song, *Catal. Today*, **111**, 74 (2006).
38. S. Rashidi, M. R. Khosravi Nikou and B. Anvaripour, *Micropor. Mesopor. Mat.*, **211**, 134 (2015).
39. D. M. Ruthven, Principles of Adsorption and Adsorption Process, Wiley, New York (1984).
40. E. I. Unuabonah, K. O. Adebowale and B. I. Olu-Owolabi, *J. Hazard. Mater.*, **144**, 386 (2007).
41. W. J. Weber, A. M. Asce and J. C. Morris, *J. Sanitary Eng. Division: Proc. Am. Soc. Civil Engineers*, **89**, 31 (1963).
42. B. Y. Ji, F. Shao, G. J. Hu, S. R. Zheng, Q. M. Zhang and Z. Y. Xu, *J. Hazard. Mater.*, **161**, 81 (2009).
43. F.-C. Wu, R.-L. Tseng and R.-S. Juang, *Chem. Eng. J.*, **153**, 1 (2009).
44. X. Han, H. F. Lin and Y. Zheng, *Can. J. Chem. Eng.*, **93**, 538 (2015).
45. C. Cheng, J. Deng, B. Lei, A. He, X. Zhang, L. Ma, S. Li and C. S. Zhao, *J. Hazard. Mater.*, **263**, 467 (2013).